

Microwave spectroscopy of spin-orbit coupled states: energy detuning versus interdot coupling modulation

G. Giavaras¹ and Yasuhiro Tokura^{1,2}

¹*Faculty of Pure and Applied Sciences, University of Tsukuba, Tsukuba 305-8571, Japan*

²*Tsukuba Research Center for Energy Materials Science (TREMS), Tsukuba 305-8571, Japan*

We study the AC field induced current peaks of a spin blockaded double quantum dot with spin-orbit interaction. The AC field modulates either the interdot tunnel coupling or the energy detuning, and we choose the AC field frequency range to induce two singlet-triplet transitions giving rise to two current peaks. We show that for a large detuning the two current peaks can be significantly stronger when the AC field modulates the tunnel coupling, thus making the detection of the spin-orbit gap more efficient. We also demonstrate the importance of the time dependence of the spin-orbit interaction.

I. INTRODUCTION

The singlet-triplet states of two electron spins in tunnel-coupled quantum dots can be used to define spin-qubits in semiconductor devices.^{1,2} In the presence of a strong spin-orbit interaction (SOI) an applied AC electric field can give rise to singlet-triplet transitions and spin resonance can be achieved.^{3,4} In a double quantum dot which is tuned to the spin blockade regime,⁵ the transitions can be probed by the AC induced current peaks. It has been experimentally demonstrated that the two-spin energy spectra can be extracted by examining the magnetic field dependent position of the current peaks.^{3,4} The exchange energy, the strength of the SOI, as well as the g -factors of the quantum dots can then be estimated. Microwave spectroscopy has also been performed for the investigation of charge qubits,^{6,7} as well as other hybrid spin systems.^{8–10} Charge localization in quantum dot systems can be controlled with AC fields,^{11–13} while various important parameters of the spin and/or charge dynamics can be extracted from AC induced interference patterns.^{14–17}

In this work, we study the current through a double dot (DD) for two different cases of the AC electric field; in the first case the AC field modulates the interdot tunnel coupling of the DD, and in the second case the AC field modulates the energy detuning of the DD. We consider a specific energy configuration and AC frequency range which involve two SOI coupled singlet-triplet states, and a third state with (mostly) triplet character. The two SOI-coupled singlet-triplet states form an anticrossing point,^{3,4,18,19} and in this work we focus on this point.

Specifically, we perform electronic transport calculations and demonstrate that for a large energy detuning the tunnel coupling modulation results in stronger AC-induced current peaks than the corresponding peaks induced by the detuning modulation. The stronger peaks can offer a significant advantage when the spectroscopy of the coupled spin system is performed by monitoring the magnetic field dependence of the position of the peaks. When the peaks are suppressed no reliable information can be extracted.

The tunnel coupling modulation offers a similar ad-

vantage when the transitions involve only the two states forming the anticrossing point.²⁰ This finding together with the results of the present work demonstrate that modulating the tunnel coupling of a DD with an AC electric field is a robust method to perform spectroscopy of spin-orbit coupled states. Furthermore, in the present work, we explore the time dependent role of the SOI, and specify the regime in which this time dependence should be taken into account because it can drastically affect the AC-induced current peaks.

In some experimental works the interdot tunnel coupling has been accurately controlled and transport measurements have been performed.^{21,22} For instance, Bertrand *et al* [Ref. 22] have demonstrated that the tunnel coupling can be tuned by orders of magnitude on the nanosecond time scale. Therefore, our theoretical findings could be tested with existing semiconductor technology.

II. DOUBLE QUANTUM DOT MODEL

We focus on the spin blockade regime⁵ for two serially tunnel-coupled quantum dots. In this regime the quantum dot 1 (dot 2) is coupled to the left (right) metallic lead and with the appropriate bias voltage current can flow through the DD when the blockade is partially or completely lifted. Each quantum dot has a single orbital level and dot 2 is lower in energy by an amount equal to the charging energy which is assumed to be much larger than the tunnel coupling. Consequently, for the appropriate bias voltage a single electron can be localized in dot 2 during the electronic transport process.⁵ If we use the notation (n, m) to indicate n electrons on the dot 1 and m electrons on the dot 2 then electronic transport process through the DD takes place via the charge cycle: $(0, 1) \rightarrow (1, 1) \rightarrow (0, 2) \rightarrow (0, 1)$. For the DD system there are in total six two-electron states but in the spin blockade regime the double occupation on dot 1 can be ignored because it lies much higher in energy and does not affect the dynamics. Therefore, the relevant two-electron states are the triplet states $|T_+\rangle = c_{1\uparrow}^\dagger c_{2\uparrow}^\dagger |0\rangle$, $|T_-\rangle = c_{1\downarrow}^\dagger c_{2\downarrow}^\dagger |0\rangle$, $|T_0\rangle = (c_{1\uparrow}^\dagger c_{2\downarrow}^\dagger + c_{1\downarrow}^\dagger c_{2\uparrow}^\dagger) |0\rangle / \sqrt{2}$ and the two singlet states

$|S_{02}\rangle = c_{2\uparrow}^\dagger c_{2\downarrow}^\dagger |0\rangle$, $|S_{11}\rangle = (c_{1\uparrow}^\dagger c_{2\downarrow}^\dagger - c_{1\downarrow}^\dagger c_{2\uparrow}^\dagger) |0\rangle / \sqrt{2}$. The fermionic operator $c_{i\sigma}^\dagger$ creates an electron on dot $i = 1, 2$ with spin $\sigma = \uparrow, \downarrow$, and $|0\rangle$ denotes the vacuum state. In this singlet-triplet basis the DD Hamiltonian²⁰ is

$$\begin{aligned} H_{\text{DD}} = & \Delta[|T_-\rangle\langle T_-| - |T_+\rangle\langle T_+|] - \delta|S_{02}\rangle\langle S_{02}| \\ & - \sqrt{2}T_c|S_{11}\rangle\langle S_{02}| + \Delta^-|S_{11}\rangle\langle T_0| + \text{H.c.} \\ & - T_{\text{so}}[|T_+\rangle\langle S_{02}| + |T_-\rangle\langle S_{02}|] + \text{H.c.} \end{aligned} \quad (1)$$

Here, δ is the energy detuning, T_c is the tunnel coupling between the two dots, and T_{so} is the SOI-induced tunnel coupling causing a spin-flip.^{23,24} The magnetic field is denoted by B which gives rise to the Zeeman splitting $\Delta_i = g_i \mu_B B$ ($i = 1, 2$) in each quantum dot. Then $\Delta = (\Delta_2 + \Delta_1)/2$, and the Zeeman asymmetry is $\Delta^- = (\Delta_2 - \Delta_1)/2$. To a good approximation, in the transport process of a spin-blockaded DD only the $c_{2\uparrow}^\dagger|0\rangle$, $c_{2\downarrow}^\dagger|0\rangle$ single electron states are important, and H_{DD} can be also derived using a standard two-site Hubbard model.²⁵

In the present work, we consider two cases for the AC field. Specifically, in the first case the AC field modulates the energy detuning of the DD, thus we consider the following time dependence:

$$\delta(t) = \varepsilon + A_d \sin(2\pi ft), \quad (2)$$

where A_d is the AC amplitude and f is the AC frequency. The constant value of the detuning is denoted by ε . In the second case, the AC field modulates the interdot tunnel coupling, thus we assume the time dependent terms

$$\begin{aligned} T_c(t) &= t_c + A_b \sin(2\pi ft), \\ T_{\text{so}}(t) &= t_{\text{so}} + x_{\text{so}} A_b \sin(2\pi ft). \end{aligned} \quad (3)$$

The AC amplitude is A_b and in general $A_b \neq A_d$. For most calculations we assume that $x_{\text{so}} = t_{\text{so}}/t_c$, so at any time the ratio $T_{\text{so}}(t)/T_c(t)$ is a time independent constant equal to x_{so} . We also address the case where $x_{\text{so}} \neq t_{\text{so}}/t_c$, but for simplicity we assume no phase difference between the tunnel couplings $T_c(t)$ and $T_{\text{so}}(t)$. For the numerical calculations the DD parameters are taken to be $t_c = 0.2$ meV, $t_{\text{so}} = 0.02$ meV, $g_1 = 2$ and $g_2 = 2.4$. The basic conclusions of this work are general enough and not specific to these numbers.

III. RESULTS

In this section we present the basic results of our work. We determine the AC induced current for each case of the two AC fields Eq. (2) and Eq. (3). The DD eigenenergies E_i satisfy $H_{\text{DD}}|\psi_i\rangle = E_i|\psi_i\rangle$ with $A_d = A_b = 0$, and are shown in Fig. 1(a) at $B = 1$ T. When $t_{\text{so}} = 0$ and $g_1 = g_2$ singlet and triplet states are uncoupled. The energy levels E_2 , E_3 and E_4 correspond to the pure triplet states $|T_+\rangle$, $|T_0\rangle$ and $|T_-\rangle$ respectively. These levels are detuning independent and are Zeeman-split due to the applied magnetic field. The energy levels E_1 , E_5 correspond to

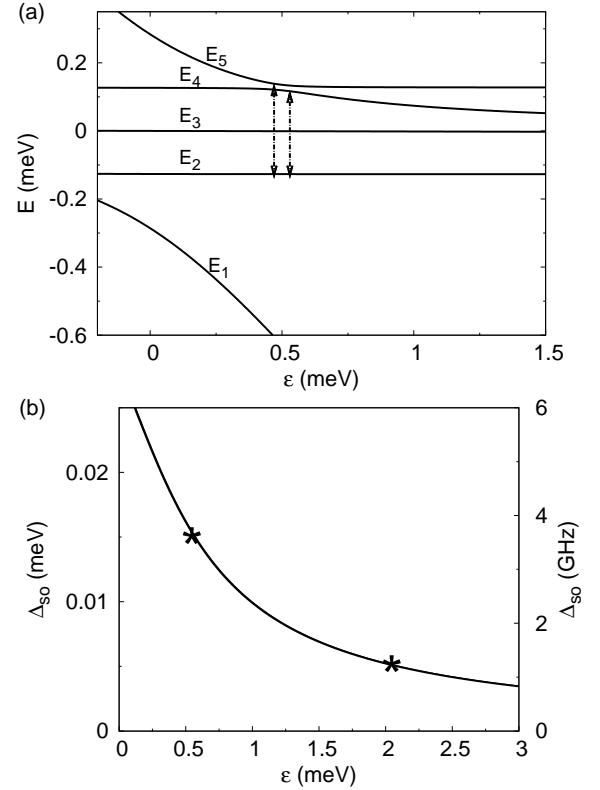


FIG. 1: (a) Two-electron eigenenergies as a function of the energy detuning for the magnetic field $B = 1$ T. The levels E_4 , E_5 anticross at $\varepsilon = 0.5$ meV due to the spin-orbit interaction. The two vertical arrows indicate possible transitions which can be induced by the AC fields defined in the main text Eq. (2) and Eq. (3). (b) Spin-orbit gap ($\Delta_{\text{so}} = E_5 - E_4$ at the anticrossing point) as a function of the detuning. In this case the magnetic field is detuning dependent. The AC induced current is computed for the marked points.

pure singlet states which are $|S_{11}\rangle$, $|S_{02}\rangle$ hybridized due to the tunnel coupling t_c and are independent of the field as can be seen from H_{DD} . Importantly, the singlet levels E_1 , E_5 define a two-level system and for a fixed t_c the hybridization is controlled by the energy detuning. The two levels E_1 , E_5 anticross at $\varepsilon = 0$ where the hybridization is maximum. This is the only anticrossing point in the energy spectrum for $t_{\text{so}} = 0$. However, according to H_{DD} when $t_{\text{so}} \neq 0$ the polarized triplets $|T_\pm\rangle$ couple to the singlet state $|S_{02}\rangle$. Therefore, as seen in Fig. 1, at $\varepsilon \approx 0.5$ meV the levels E_4 and E_5 form an anticrossing point due to the SOI. Another SOI-induced anticrossing point is formed at $\varepsilon < 0$ between the energy levels E_1 and E_2 , but here we consider $\varepsilon > 0$ and as in the experiments^{3,26-28} we take $t_{\text{so}} < t_c$.

Because of the SOI ($t_{\text{so}} \neq 0$) and the difference in the g -factors ($g_1 \neq g_2$) the DD eigenstates $|\psi_i\rangle$ are hybridized singlet-triplet states and can be written in the general form

$$|\psi_i\rangle = \alpha_i|S_{11}\rangle + \beta_i|T_+\rangle + \gamma_i|S_{02}\rangle + \zeta_i|T_-\rangle + \eta_i|T_0\rangle. \quad (4)$$

The coefficients denoted by Greek letters determine the character of the states, and are sensitive to the detuning.

One method to probe the SOI anticrossing point is to focus on the AC frequency range $0 < hf \lesssim E_5 - E_4$ and determine the position of the AC induced current peak. This method has been theoretically studied in Ref. 20. Another method to probe the anticrossing point is to focus on the AC frequency range $E_4 - E_2 \lesssim hf \lesssim E_5 - E_2$, and determine the positions of the two AC induced current peaks. The present work is concerned with the latter method and the main subject of the present work is to compare the current peaks induced separately by the two AC fields; the tunnel barrier modulation and energy detuning modulation. In Ref. 3 both methods have been experimentally investigated under the assumption that the AC field modulates the energy detuning of the DD. The case where the AC field modulates simultaneously the interdot tunnel coupling and the energy detuning might be experimentally relevant,²⁹ but this case is not pursued in the present work.

In Fig. 1 the SOI anticrossing is formed at $\varepsilon \approx 0.5$ meV for $B = 1$ T. A lower magnetic field shifts the SOI anticrossing point at larger detuning, and the degree of hybridization due to the SOI decreases. The reason is that as ε increases the $|S_{02}\rangle$ character in the original singlet state ($t_{so} = 0$) is gradually replaced by the $|S_{11}\rangle$ character. As a result, the SOI gap $\Delta_{so} = E_5 - E_4$, defined at the anticrossing point, decreases with ε as shown in Fig. 1(b). For the parameters considered in this work, the SOI gap can be analytically determined from the expression³⁰ $\Delta_{so} = 2t_{so}\sqrt{(1 - \cos\theta)/2}$, with $\theta = \arctan(2\sqrt{2}t_c/\varepsilon)$.

In our previous work²⁰ we examined the transitions between the two singlet-triplet states $|\psi_4\rangle$ and $|\psi_5\rangle$, whose energy levels form the SOI anticrossing point (Fig. 1). These transitions give rise to one current peak which is suppressed near the anticrossing point, in agreement with an experimental study.³ In the present work, we focus on the transitions between the two pairs of states $|\psi_5\rangle$ and $|\psi_2\rangle$ as well as $|\psi_4\rangle$ and $|\psi_2\rangle$. Here, $|\psi_4\rangle$ and $|\psi_5\rangle$ are strongly hybridized singlet-triplet states, whereas $|\psi_2\rangle$ has mostly triplet character provided the detuning is large.

We compute the AC-induced current flowing through the double dot within the Floquet-Markov density matrix equation of motion.^{31,32} In this approach we treat the time dependence of the AC field exactly, taking advantage of the fact that the DD Hamiltonian is time periodic and thus it can be expanded in a Fourier series. The model uses for the basis states of the DD density matrix the periodic Floquet modes,³³ and consequently it is applicable for any amplitude of the AC field. In most calculations we take the parameter $x_{so} = 0.1$ unless otherwise specified.

To study the AC current spectra we choose two values for the energy detuning ε (2, 0.5 meV), and determine the magnetic field at which $|\psi_4\rangle$ and $|\psi_5\rangle$ anticross. At this specific field we plot in Fig. 2 the AC-induced current as

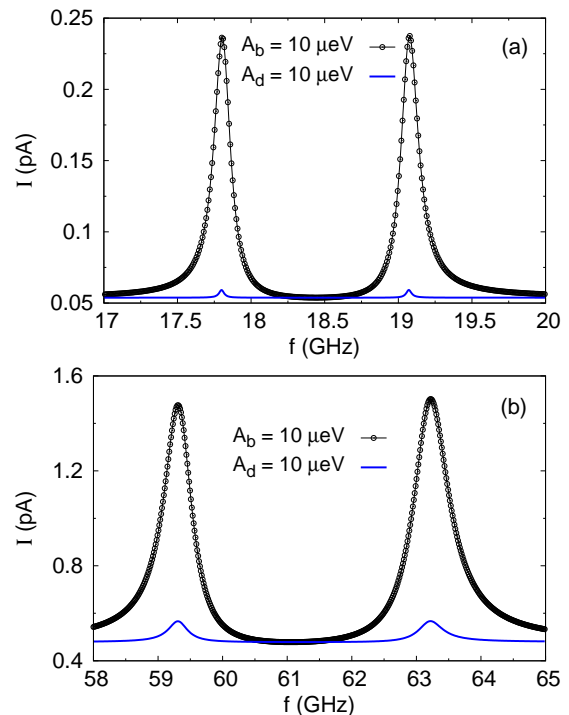


FIG. 2: Current as a function of AC frequency, when the AC field modulates the tunnel barrier with the AC amplitude $A_b = 10 \mu\text{eV}$, and the energy detuning with $A_d = 10 \mu\text{eV}$. The constant value of the detuning is $\varepsilon = 2, 0.5$ meV and the corresponding magnetic field is $B = 0.3, 1$ T for (a) and (b) respectively. These fields define the singlet-triplet anticrossing point for each value of the detuning.

a function of the AC frequency. As the energy detuning decreases the magnetic field defining the corresponding anticrossing point increases. This in turn means that the AC frequency has to increase to satisfy the corresponding resonance condition $hf = E_5 - E_2$ (or $hf = E_4 - E_2$). This increase in the frequency explains the different frequency range in Fig. 2. Furthermore, the off-resonant current is larger for $\varepsilon = 0.5$ meV due to the stronger SOI hybridization.²⁵

In the two cases shown in Fig. 2 two peaks are formed; one peak is due to the transition between the eigenstates $|\psi_2\rangle$ and $|\psi_4\rangle$, and the second peak is due to the transition between $|\psi_2\rangle$ and $|\psi_5\rangle$. Therefore, the distance between the centres of the two peaks is equal to the singlet-triplet energy splitting $E_5 - E_4$. For the specific choice of magnetic field this energy splitting is equal to the SOI gap of the anticrossing point. For example, for $\varepsilon = 0.5$ meV the gap is $\Delta_{so} \approx 3.5$ GHz, and for $\varepsilon = 2$ meV the gap is $\Delta_{so} \approx 1.1$ GHz. These numbers are in agreement with those derived from the exact energies of the time independent part of the Hamiltonian H_{DD} . According to Fig. 2, for a given energy detuning and driving field the two peaks are almost identical. This is due to the fact, that at the anticrossing point the states $|\psi_4\rangle, |\psi_5\rangle$ have identical characters when the driving field is off, and the relevant transition rates are almost equal. In contrast,

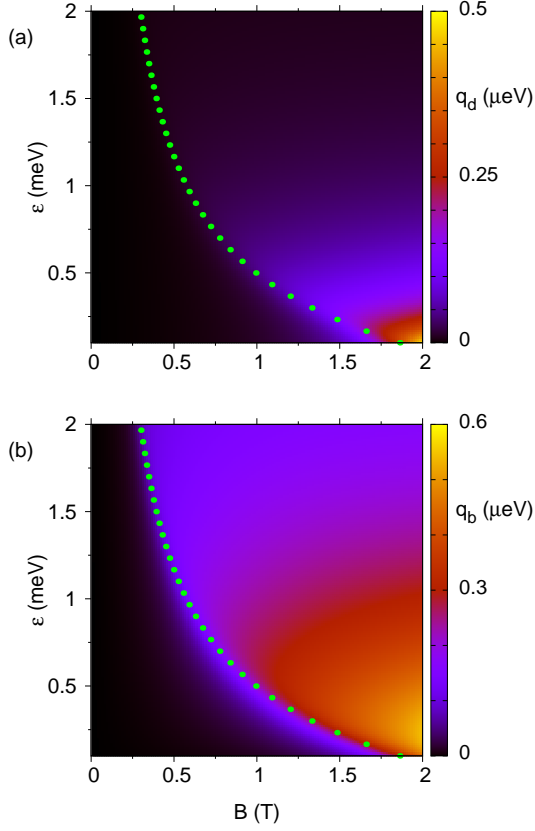


FIG. 3: (a) Absolute value of the coupling parameter q_d as a function of the energy detuning and magnetic field for the AC amplitude $A_d = 10 \mu\text{eV}$. The dotted curve defines the anticrossing point for each ε and B . (b) The same as (a) but for q_b with $A_b = 10 \mu\text{eV}$.

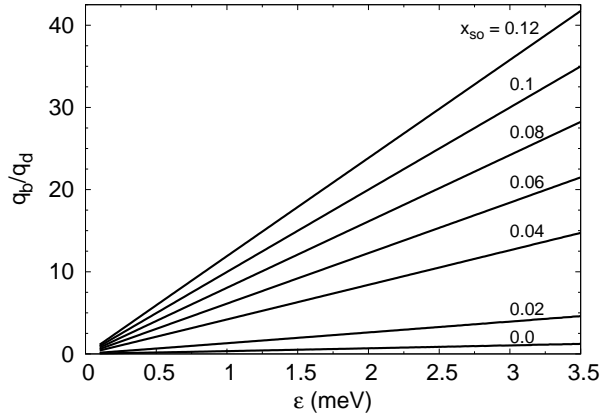


FIG. 4: The ratio q_b/q_d defined in Eq. (9) as a function of detuning for different values of x_{so} and $A_d = A_b$.

away from the anticrossing point the two peaks can be very different.³³

The results in Fig. 2 demonstrate that the two driving fields Eq. (2) and Eq. (3) induce different peak magnitudes. Specifically, the peaks due to the tunnel barrier modulation are stronger than those due to the detuning

modulation. As an example, for $\varepsilon = 0.5 \text{ meV}$ [Fig. 2(b)] the tunnel barrier modulation induces a relative peak height of about 1 pA, whereas the relative peak height is only 0.1 pA for the energy detuning modulation. Some insight into this interesting behavior can be obtained by inspecting the time-scale (“Rabi” frequency) of the coherent transitions between the eigenstates $|\psi_2\rangle$ and $|\psi_4\rangle$. When the AC field modulates the tunnel coupling, the transitions can be studied within the exact Floquet eigenvalue problem, but for simplicity we here employ an approximate approach.²⁰ This two-level approach gives the transition frequency q_b/h , with

$$q_b = \frac{hf h_{24}^b}{(h_{22}^b - h_{44}^b)} J_1 \left(\frac{A_b(h_{22}^b - h_{44}^b)}{hf} \right), \quad (5)$$

where $J_1(r)$ is a Bessel function of the first kind, and the argument is $r = A_b(h_{22}^b - h_{44}^b)/hf$, with $hf = E_4 - E_2$ and

$$h_{ij}^b = -\gamma_j(\sqrt{2}\alpha_i + x_{\text{so}}\beta_i + x_{\text{so}}\zeta_i) - \gamma_i(\sqrt{2}\alpha_j + x_{\text{so}}\beta_j + x_{\text{so}}\zeta_j), \quad i, j = 2, 4 \quad (6)$$

When the AC field modulates the energy detuning the time-scale of the coherent transitions between the eigenstates $|\psi_2\rangle$ and $|\psi_4\rangle$ is approximately q_d/h . The coupling parameter q_d is found by q_b with the replacements $A_b \rightarrow A_d$ and $h_{ij}^b \rightarrow h_{ij}^d$, where

$$h_{ij}^d = -\gamma_i\gamma_j, \quad i, j = 2, 4 \quad (7)$$

In general, q_b can be very different from q_d , even when $A_b = A_d$. Therefore, the two driving fields are expected to induce current peaks with different width and height.

To quantify the two parameters q_b, q_d we plot in Fig. 3 q_b, q_d , as a function of the energy detuning and the magnetic field. Here, $A_d = A_b = 10 \mu\text{eV}$, and $hf = E_4 - E_2$ [in Eq. (5)] is magnetic field as well as detuning dependent, and is determined by the energies of H_{DD} . If we denote by B_{an} the field at which the anticrossing point is formed, then as seen in Fig. 3 both q_b and q_d are large for $B > B_{\text{an}}$, but vanishingly small for $B \ll B_{\text{an}}$. The reason is that the state $|\psi_4\rangle$ is singlet-like for $B > B_{\text{an}}$, but triplet-like for $B < B_{\text{an}}$, whereas $|\psi_2\rangle$ has mostly triplet character independent of B , provided ε is away from zero. Transitions between triplet-like states are in general slow leading to vanishingly small q_b, q_d for $B \ll B_{\text{an}}$. In contrast, if we choose $hf = E_5 - E_2$, then both q_b and q_d are large for $B < B_{\text{an}}$. For large enough detuning where the two spins are in the Heisenberg regime, the exchange energy is approximately $2t_c^2/\varepsilon$ therefore B_{an} satisfies $(g_1 + g_2)\mu_B B_{\text{an}}/2 \approx 2t_c^2/\varepsilon$.

Most importantly Fig. 3 demonstrates that $q_b > q_d$ when $\varepsilon \gtrsim 0.2 \text{ meV}$. To understand this result we focus on the anticrossing point where $r < 1$, then from Eq. (5) $q_b \approx h_{24}^b A_b/2$ because $J_1(r) \approx r/2$, and similarly $q_d \approx h_{24}^d A_d/2$. Moreover, away from zero detuning the state $|\psi_2\rangle$ has mostly triplet character, therefore

$$h_{24}^b \approx -\gamma_4(\sqrt{2}\alpha_2 + x_{\text{so}}\beta_2) - \gamma_2(\sqrt{2}\alpha_4 + x_{\text{so}}\zeta_4), \quad (8)$$

and the ratio q_b/q_d is

$$\frac{q_b}{q_d} = \frac{A_b}{A_d} \left(\sqrt{2} \frac{\alpha_2}{\gamma_2} + x_{so} \frac{\beta_2}{\gamma_2} + \sqrt{2} \frac{\alpha_4}{\gamma_4} + x_{so} \frac{\zeta_4}{\gamma_4} \right). \quad (9)$$

As ε increases $\beta_2 \rightarrow 1$, $\gamma_2 \ll 1$ and, considering absolute values, the second term in Eq. (9) dominates

$$\frac{\beta_2}{\gamma_2} \gg \frac{\alpha_2}{\gamma_2}, \frac{\alpha_4}{\gamma_4}, \frac{\zeta_4}{\gamma_4}. \quad (10)$$

Consequently, q_b can be much greater than q_d , especially at large ε , and for a fixed tunnel coupling t_c the exact value of the ratio q_b/q_d depends sensitively on x_{so} . This demonstrates the importance of the time dependence of the spin-orbit coupling. The conclusions derived from the parameters q_b , q_d assume that there is no ‘multi-level’ interference and only the levels E_i , E_j satisfying $hf = |E_i - E_j|$ are responsible for the current peaks. The approximate results are more accurate when the argument r of the Bessel function is kept small.

To examine the x_{so} -dependence, we consider $A_b = A_d$ and plot in Fig. 4 the ratio q_b/q_d versus the detuning at the anticrossing point, and for different values of x_{so} . By increasing ε and for large values of x_{so} the coupling parameters q_b , q_d can differ by over an order of magnitude; $q_b/q_d > 10$. This leads to (very) different current peaks with the tunnel barrier modulation inducing stronger peaks. The special value $x_{so} = 0$ corresponds to a time independent SOI tunnel coupling [see Eq. (3)], and the special value $x_{so} = 0.1$ corresponds to a time independent ratio $T_{so}/T_c = 0.1$. Although, the ratio q_b/q_d can be computed at any ε , the regime of small ε (< 0.2 meV) is not particularly interesting in this work. The reason is that with decreasing ε the character of the state $|\psi_2\rangle$ changes from triplet-like to singlet-triplet, which eventually becomes approximately equally populated to $|\psi_4\rangle$ and $|\psi_5\rangle$. Therefore, the current peaks induced by both driving fields are suppressed even when q_b or q_d is large. In Fig. 4 the maximum value of the detuning is chosen to give $\varepsilon/t_c \approx 17.5$ which can be easily achieved in double quantum dots. Some experiments^{1,3,4} have reported values greater than $\varepsilon/t_c \approx 100$, thus q_b can be even two orders of magnitude greater than q_d .

According to the above analysis if $q_b/q_d \approx 1$ then the current peaks induced by the two driving fields should approximately display the same characteristics. As an example, consider the two sets of current peaks shown in Fig. 2 both for $x_{so} = 0.1$ and $\varepsilon = 2$ meV, $\varepsilon = 0.5$ meV respectively. Focusing on $x_{so} = 0.1$ in Fig. 4, we see that at $\varepsilon = 2$ meV $q_b/q_d \approx 19$ and at $\varepsilon = 0.5$ meV $q_b/q_d \approx 4.9$. These numbers suggest that if at $\varepsilon = 2$ meV we choose for the AC amplitudes the ratio $A_b/A_d \approx 1/19$ then the detuning and the barrier modulation should induce approximately the same peak characteristics. Likewise at $\varepsilon = 0.5$ meV the ratio should be $A_b/A_d \approx 1/4.9$. These arguments are quantified in Fig. 5 where we plot the current peaks for the two driving fields for different AC amplitudes satisfying the condition $q_b/q_d \approx 1$. The

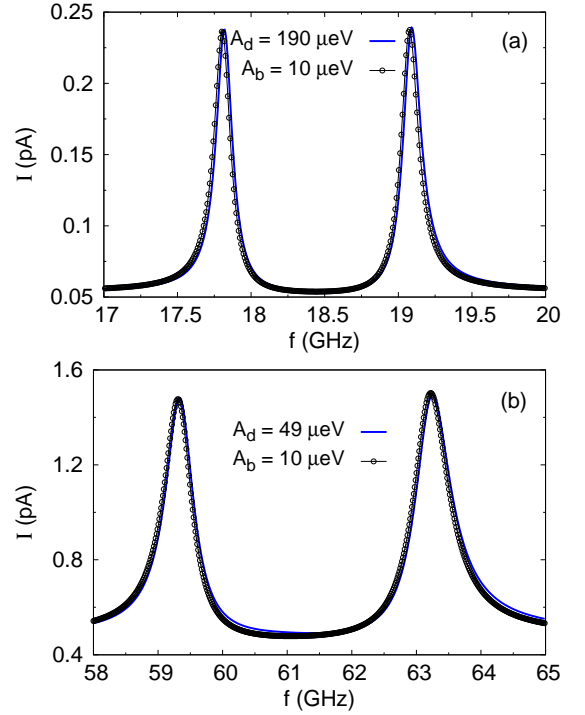


FIG. 5: As in Fig. 2, but (a) $A_b = 10 \mu\text{eV}$ and $A_d = 19A_b$, (b) $A_b = 10 \mu\text{eV}$ and $A_d = 4.9A_b$. The value of A_d is chosen so that to approximately induce the same current peaks as those induced by A_b .

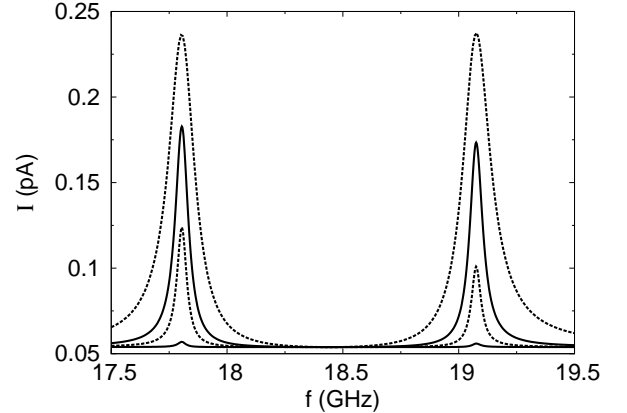


FIG. 6: Current as a function of AC frequency, when the AC field modulates the tunnel barrier, with the AC amplitude $A_b = 10 \mu\text{eV}$. The detuning is $\varepsilon = 2$ meV and from the upper to the lower curve the parameter $x_{so} = 0.1, 0.04, 0.02, 0$.

results confirm that the induced current peaks display approximately the same characteristics.

Inducing strong current peaks can be advantageous in order to perform spectroscopy of the singlet-triplet levels and extract the SOI anticrossing gap. However, an important aspect is that the SOI gap cannot be extracted from the positions of the current peaks at arbitrary large AC amplitudes. In particular, by increasing the AC amplitude the two peaks start to overlap and eventually

the resonant pattern of the current changes drastically.³³ Therefore, the distance between the two peaks cannot accurately predict the SOI gap. This effect has been theoretically studied for the case of a time dependent energy detuning,³³ and it can be readily shown that similar trends occur for a time dependent tunnel coupling. The driving regime where the two current peaks strongly overlap is not considered in the present work, since it is not appropriate for the spectroscopy of the SOI gap.

Finally, in Fig. 6 we plot the current peaks when the AC field modulates the tunnel barrier with the amplitude $A_b = 10 \mu\text{eV}$ and the constant detuning $\varepsilon = 2 \text{ meV}$. With decreasing x_{so} the two peaks gradually weaken and for $x_{\text{so}} = 0$ the peaks are vanishingly small; for this value the peaks are of the same order as the peaks induced by the detuning modulation with the same amplitude $A_d = 10 \mu\text{eV}$ (for clarity these peaks are not shown). The small difference between the left and the right peaks, for example when $x_{\text{so}} = 0.02$, can be understood by inspecting the different values of q_b [Eq. (5)] which involve different matrix elements and frequencies. The overall trends indicate the important role of the time dependent spin-orbit term and are consistent with the results shown in Fig. 4. As x_{so} decreases the coupling parameter q_b decreases too, thus the time scale of the singlet-triplet transitions becomes longer leading to smaller peaks. Moreover, by decreasing x_{so} , q_b becomes approximately equal to q_d , therefore the tunnel barrier modulation and the detuning modulation

result in approximately the same current peaks.

IV. SUMMARY

In summary, we considered a double quantum dot in the spin blockade regime and studied the AC induced current peaks for a specific energy configuration which involves two hybridized singlet-triplet states as well as a third state with mostly triplet character. The two AC induced transitions which rely on the spin-orbit interaction, result in two current peaks. We found that for a large energy detuning the two peaks are stronger when the time periodic field modulates the interdot tunnel coupling (barrier) instead of the energy detuning. We demonstrated that a time dependence in the spin-orbit coupling can significantly modify the peak characteristics, and should be taken into account even when the actual spin-orbit coupling is small. Our work suggests an efficient way of probing the spin-orbit energy gap in two-spin states based on transport measurements.

ACKNOWLEDGEMENT

Part of this work was supported by CREST JST (JPMJCR15N2), and by JSPS KAKENHI (18K03479).

-
- ¹ J. R. Petta, A. C. Johnson, J. M. Taylor, E. A. Laird, A. Yacoby, M. D. Lukin, C. M. Marcus, M. P. Hanson, and A. C. Gossard, *Science* **309**, 2180 (2005).
 - ² J. J. L. Morton, and B. W. Lovett, *Annu. Rev. Condens. Matter Phys.* **2**, 189 (2011).
 - ³ K. Ono, G. Giavaras, T. Tanamoto, T. Ohguro, X. Hu, and F. Nori, *Phys. Rev. Lett.* **119**, 156802 (2017).
 - ⁴ S. Nadj-Perge, V. S. Pribiag, J. W. G. van den Berg, K. Zuo, S. R. Plissard, E. P. A. M. Bakkers, S. M. Frolov, and L. P. Kouwenhoven, *Phys. Rev. Lett.* **108**, 166801 (2012).
 - ⁵ K. Ono, D. G. Austing, Y. Tokura, and S. Tarucha, *Science* **297**, 1313 (2002).
 - ⁶ T. Hayashi, T. Fujisawa, H. D. Cheong, Y. H. Jeong, and Y. Hirayama, *Phys. Rev. Lett.* **91**, 226804 (2003).
 - ⁷ Z. V. Penfold-Fitch, F. Sfigakis, and M. R. Buitelaar, *Phys. Rev. Applied* **7**, 054017 (2017).
 - ⁸ B. C. Wang, G. Cao, H. O. Li, M. Xiao, G. C. Guo, X. Hu, H. W. Jiang, and G. P. Guo, *Phys. Rev. Applied* **8**, 064035 (2017).
 - ⁹ X. C. Yang, G. X. Chan, and X. Wang, *Phys. Rev. A* **98**, 032334 (2018).
 - ¹⁰ W. Song, T. Du, H. Liu, M. B. Plenio, and J. Cai, *Phys. Rev. Applied* **12**, 054025 (2019).
 - ¹¹ E. Paspalakis and A. Terzis, *J. Appl. Phys.* **95**, 1603 (2004).
 - ¹² A. Terzis and E. Paspalakis, *J. Appl. Phys.* **97**, 023523 (2005).
 - ¹³ C. E. Creffield and G. Platero, *Phys. Rev. B* **65**, 113304 (2002).
 - ¹⁴ S. N. Shevchenko, S. Ashhab, and F. Nori, *Phys. Rep.* **492**, 1 (2010).
 - ¹⁵ S. N. Shevchenko, S. Ashhab, and F. Nori, *Phys. Rev. B* **85**, 094502 (2012).
 - ¹⁶ F. Gallego-Marcos, R. Sanchez, and G. Platero *J. Appl. Phys.* **117**, 112808 (2015).
 - ¹⁷ A. Chatterjee, S. N. Shevchenko, S. Barraud, R. M. Otxoa, F. Nori, J. J. L. Morton, and M. F. Gonzalez-Zalba, *Phys. Rev. B* **97**, 045405 (2018).
 - ¹⁸ S. Takahashi, R. S. Deacon, K. Yoshida, A. Oiwa, K. Shibata, K. Hirakawa, Y. Tokura, and S. Tarucha, *Phys. Rev. Lett.* **104**, 246801 (2010).
 - ¹⁹ Y. Kanai, R. S. Deacon, S. Takahashi, A. Oiwa, K. Yoshida, K. Shibata, K. Hirakawa, Y. Tokura, and S. Tarucha, *Nature Nanotechnology* **6**, 511 (2011).
 - ²⁰ G. Giavaras and Y. Tokura, *Phys. Rev. B* **99**, 075412 (2019).
 - ²¹ T. H. Oosterkamp, T. Fujisawa, W. G. van der Wiel, K. Ishibashi, R. V. Hijman, S. Tarucha, and L. P. Kouwenhoven, *Nature (London)* **395**, 873 (1998).
 - ²² B. Bertrand, H. Flentje, S. Takada, M. Yamamoto, S. Tarucha, A. Ludwig, A. D. Wieck, C. Buerle, and T. Meunier, *Phys. Rev. Lett.* **115**, 096801 (2015).
 - ²³ F. Mireles and G. Kirczenow, *Phys. Rev. B* **64**, 024426 (2001).
 - ²⁴ H. Pan and Y. Zhao, *J. Appl. Phys.* **111**, 083703 (2012).
 - ²⁵ G. Giavaras, N. Lambert, and F. Nori, *Phys. Rev. B* **87**, 115416 (2013).
 - ²⁶ S. J. Chorley, G. Giavaras, J. Wabnig, G. A. C. Jones, C.

- G. Smith, G. A. D. Briggs, and M. R. Buitelaar, Phys. Rev. Lett. **106**, 206801 (2011).
- ²⁷ G. Xu *et al.*, Appl. Phys. Express **13**, 065002 (2020).
- ²⁸ M. Marx, J. Yoneda, T. Otsuka, K. Takeda, Y. Yamaoka, T. Nakajima, S. Li, A. Noiri, T. Kadera, and S. Tarucha, Jpn. J. Appl. Phys. **58**, SBBI07 (2019).
- ²⁹ T. Nakajima, M. R. Delbecq, T. Otsuka, S. Amaha, J. Yoneda, A. Noiri, K. Takeda, G. Allison, A. Ludwig, A. D. Wieck, X. Hu, F. Nori, and S. Tarucha, Nature Communications **9**, 2133 (2018).
- ³⁰ D. Stepanenko, M. Rudner, B. I. Halperin, and D. Loss, Phys. Rev. B **85**, 075416 (2012).
- ³¹ M. Grifoni and P. Hänggi, Phys. Rep. **304**, 229 (1998).
- ³² S. Kohler, J. Lehmann, and P. Hänggi, Phys. Rep. **406**, 379 (2005).
- ³³ G. Giavaras and Y. Tokura, Phys. Rev. B **100**, 195421 (2019).